Calculation of helium photoionization with excitation including angular distribution and resonance structure

S. Salomonson,* S. L. Carter, and H. P. Kelly
Department of Physics, University of Virginia, Charlottesville, Virginia 22901
(Received 3 May 1988; revised manuscript received 28 November 1988)

A nine-channel coupled-equation calculation for photoionization of the $1s^2$ ground state of He is performed within the framework of many-body perturbation theory. Partial cross sections for leaving the ion in $1s$, $2s$, $2p$, $3s$, $3p$, and $3d$ levels are obtained together with the angular asymmetry parameter for leaving the ion in $n=2$ states. The resonance structure in the $1s$, $2s$, and $2p$ cross sections and in the $n=2$ angular asymmetry parameter due to doubly excited autoionizing states below the $n=3$ threshold is calculated. Also, parameters describing the resonances in the $1s$ cross section below the $n=2$ threshold are obtained.

I. INTRODUCTION

Photoionization with excitation and double-electron photoionization are important components of the absorption of light by atoms, which was pointed out by Wuilleumier and Krause[1] many years ago. For He these processes account for about 10% of the total photoabsorption over a wide range of energies.[2]

The first measurement of photoionization with excitation for helium was made by Samson[3] using photoelectron spectroscopy. Krause and Wuilleumier[4] also measured the angular distribution in order to resolve the degenerate $2s$ and $2p$ ionic levels. This was measured over a broader energy range by Bizau *et al.*,[5] Schmidt *et al.*,[6] and Lindle and co-workers[7,8] using synchrotron radiation. To resolve the $2p$ and $2s$ levels from the measured angular distribution, one has to rely on theoretical calculations of the angular asymmetry parameter for leaving the ion in the $2p$ level. An experiment that directly separates the $2s$ and $2p$ levels was performed by Woodruff and Samson[9,10] monitoring the 304-Å fluorescence light with and without an applied electric field that causes mixing between the $2s$ and $2p$ levels.

Relatively few calculations have been performed of cross sections for photoionization with excitation of He.[11–16] None of them include resonance structure, caused by doubly excited autoionizing states. On the other hand, there exist a number of calculations giving the energy positions and widths[17–24] of the autoionizing states relevant for photoionization with excitation. Recently Burkov *et al.*[25] have calculated cross sections and angular asymmetry for photoionization with excitation to $n=2$ states.

Evidence for the existence of doubly excited autoionizing states in helium was found already around 1930. A brief review and references to the earlier experimental and theoretical work are given by Madden and Codling,[26] who were the first to observe doubly excited states in total photoabsorption measurements in 1963 (Refs. 26 and 27) using synchrotron radiation.

An interesting feature is the relatively large resonance structure in the cross sections for photoionization with excitation to $n=2$ levels, compared to the corresponding structure in the main channel. This was discovered experimentally by Woodruff and Samson[9,10] and confirmed by Lindle and co-workers,[7,8] who also measured the resonance structure in the angular distribution. Their findings are very challenging for theorists.

In an earlier paper[28] we presented a calculation of the ratio of the cross sections leaving the ion in the $2p$ and $2s$ levels (σ_{2p}/σ_{2s}). We confirmed the now well-established fact that σ_{2p} dominates over σ_{2s} near threshold,[6,8,10] which has been the subject of a controversy.[5,13,14] We also presented the first calculation of the resonance structure in the $n=2$ cross section ($\sigma_{2s}+\sigma_{2p}$) below the $n=3$ threshold. In the present work we give a more comprehensive presentation of our calculation of He photoionization with excitation to $n=2$ levels. We also present cross sections for excitation to $n=3$ levels. The emphasis is on the $n=2$ cross sections and the angular asymmetry, particularly in the resonance region below the $n=3$ threshold. We compare our results in this region with the experimental data of cross sections and the angular asymmetry parameter.[8,10]

Our work is based on many-body perturbation theory which is briefly outlined in Sec. II. There we mention the use of the pair equation[29] to calculate ground-state correlation to all orders and describe the coupled-integral-equation technique[30] to sum certain classes of final-state correlation effects to all orders. A close-coupling approximation is made, including the nine channels based on exact He^+ states with $n=1$, 2, and 3.

Some numerical aspects and problems related to the coupled-integral-equation technique are discussed in Sec. III. These include a problem with sharp peaking of the Coulomb matrix elements and a blocking technique used to solve the coupled equations. We also present a numerical test of the coupled-equation code within the main channel.

In Sec. IV we present numerical results for the various

channels, with emphasis on cross sections and angular asymmetry in the resonance region below the $n=3$ ionization threshold. We also present results for cross sections with the ion excited to $n=3$ levels and results about the resonances below the $n=2$ threshold. A short summary and conclusions are given in Sec. V.

II. THEORY

A. Basic formulas and perturbation theory

We use the well-known relation[31,32] between the photoionization cross section $\sigma(\omega)$ and the imaginary part of the frequency-dependent dipole polarizability $\alpha(\omega)$,

$$\sigma(\omega)=(4\pi/c)\omega\,\mathrm{Im}\alpha(\omega)\ . \tag{1}$$

Atomic units ($e=m=\hbar=4\pi\epsilon_0=1$) are used throughout this paper. The expression for $\mathrm{Im}\alpha(\omega)$ may be written in terms of dipole matrix elements $\langle\Psi_{f,j}|D_z|\Psi_i\rangle$ between the initial state and the final state of a particular channel j, leading to

$$\sigma(\omega)=\sum_j\int dE_f(8\pi\omega/ck)|\langle\Psi_{f,j}|D_z|\Psi_g\rangle|^2 \times\delta(E_g+\omega-E_{f,j})\ , \tag{2}$$

where the many-particle dipole operator D_z may be of either the length form $\sum_i z_i$ or the velocity form $(-1/\omega)\sum_i d/dz_i$.[33] The δ function restricts the summation here to channels j with continuum states degenerate with $E_g+\omega$, or in other words the summation is over all open channels. These include the different possible states for the ion, different angular momenta of the outgoing electron, and different couplings between the ion and the photoelectron. In deriving Eq. (2) we have made use of the fact that our continuum functions describing the outgoing electron have the normalization

$$P_k(r)=rR_k(r) =\sin[kr+(q/k)\ln(2kr)-(\pi/2)l+\sigma_l+\delta_l]\ , \tag{3}$$

where q is the effective charge affecting the outgoing electron, σ_l the Coulomb phase shift given by $\sigma_l=\arg[\Gamma(1-iq/k)]$, and δ_l is the residual phase shift with respect to the Coulomb wave.

The Hamiltonian H can be split into a zeroth-order approximation H_0 consisting of one-electron operators only and a correlation part V treated as a perturbation, $H=H_0+V$, where

$$V=\tfrac{1}{2}\sum_{\substack{i,j\\ i\neq j}}1/r_{ij}-\sum_i u(r_i)\ . \tag{4}$$

Here $u(r_i)$ represents a spherically symmetric one-electron potential that approximately takes the interaction with the other electrons into account.

Using a complete set of single-particle states calculated with $u(r_i)$, a diagrammatic many-body perturbation expansion[34–36] may be developed for $\alpha(\omega)$ in Eq. (1) or for the many-particle dipole-matrix elements. When calculating $\sigma(\omega)$ in terms of many-particle dipole-matrix elements, one has to include a small correction from normalization diagrams.[36]

The lowest-order diagram for the dipole-matrix element is shown in Fig. 1(a), and diagrams with one correlation interaction of Eq. (4) are shown in Figs. 1(b)–1(g). We are using the diagrammatic notation described by Lindgren and Morrison,[37] and the $1s^2$ electrons of helium are treated as belonging to an open shell in the perturbation expansion. Lines with double arrows denote the open-shell electrons ($1s$ for He) while bare lines represent either virtual or open-shell electrons. After each interaction the diagrams must represent true excitations. Diagram 1(a) represents the first-order contribution to the main channel $1skp$. In next order, as in Figs. 1(b) and 1(c), one of the outgoing lines can represent an excited bound state of He^+. These diagrams contribute to the dipole-matrix elements for photoionization with excitation, i.e, channels like $2skp$.

Correlation effects in the initial state were accounted for by the use of pair functions as described in Lindgren and Morrison.[37] Detailed equations for the pair functions and the numerical technique to solve them iteratively are described by Mårtensson.[29] With the pair functions we essentially get an exact description of a bound two-electron system, the accuracy depending on the number of partial waves used. In this work partial waves up to $l=6$ were included. The use of pair functions is not limited to two-electron systems, however, and has e.g., been used for calculations of hyperfine structure in Li and Na (Ref. 38) and in K and Rb,[39] correlation energies in Be and Ne (Ref. 40) and specific-mass shifts in Li and K.[41]

B. Coupled integral equations

The final-state correlation was taken into account by solving a system of coupled integral equations.[30] A nu-

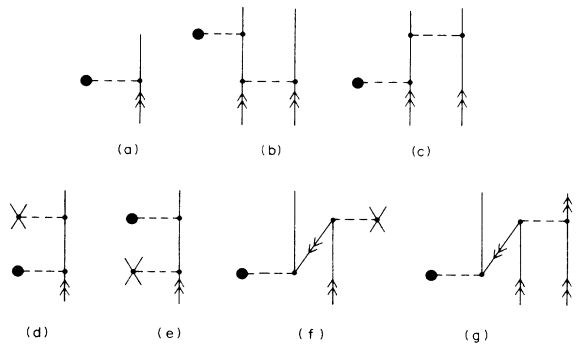

FIG. 1. First- and second-order diagrams that contribute to the dipole-matrix elements between the ground-state and the final-state wave functions. Vertical lines with double arrows denote valence electrons ($1s$ in our case) while bare vertical lines represent either virtual or (when allowed) valence electrons. The horizontal dashed lines ending with an isolated solid dot represent dipole-matrix elements and similar lines ending with a cross represent potential corrections. The other dashed lines represent the Coulomb interaction.

merically represented basis of bound and continuum orbitals was generated. The $1s$, $2s$, $3s$, $2p$, $3p$, and $3d$ orbitals were chosen to be exact states of He^+. The remaining bound and continuum orbitals were generated in the frozen-core Hartree-Fock potential from one of the ionic orbitals, with the ionic orbital and the basis orbital coupled to a ^1P state. The s and d orbitals were generated in the potential of the $2p$ orbital, the p orbitals in the potential of the $2s$ orbital, and the f orbitals in the potential of the $3d$ orbital. Projection operators[42] were used to define a Hermitian potential valid for all orbitals of a specific angular momentum. As an example, the potential for the p orbitals is

$$u=(1-P)(J^0_{2s}+\tfrac{1}{3}K^1_{2s})(1-P)\ , \tag{5}$$

where

$$P=|2p\rangle\langle 2p|+|3p\rangle\langle 3p|\ . \tag{6}$$

This gives a well-defined potential suitable for perturbation theory, and assures that the orbitals generated form a complete orthogonal basis. To represent the final state, nine channels were included: $1skp$, $2skp$, $2pks$, $2pkd$, $3skp$, $3pks$, $3pkd$, $3dkp$, and $3dkf$, where k here denotes either a bound orbital or a continuum orbital. This close-coupling approximation thus neglects higher-excited channels based on $n\geq 4$ He^+ states, including double-ionization channels.

For each channel eight bound orbitals were used, selected so that double counting between different channels was avoided. The lowest bound state was, e.g., chosen to be $3p$ in the $3skp$ channel and $4s$ in the $3pks$ channel. The continuum orbitals were represented by a mesh of 42 k values ranging from 0.05 to 14.0 a.u. Dipole-matrix elements from the correlated ground state to the basis functions representing the channels included in the final state were calculated together with Coulomb matrix elements between the final-state basis functions. Coupling between the final-state channels can be included to all orders by solving a coupled system of integral equations.[30] We are essentially performing a K-matrix calculation among the discretized channels[43] and this is shown schematically in Fig. 2. Here we let the bottom of the diagrams with the wavy line, in addition to the pair function, include the $1s^2$ zeroth-order wave function. The coupled integral equations can also be written out explicitly as

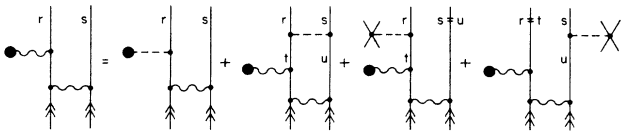

FIG. 2. Graphical representation of the coupled equations. Here the bottom of the diagrams with the wavy line in addition to the pair function includes the $1s^2$ zeroth-order wave function. The diagram on the left-hand side represents the unknown effective-dipole-matrix element from the correlated ground state to the correlated final state. The wavy dipole interaction line indicates the inclusion of the final-state correlation within the included channels.

$$\langle rs|D_{\rm eff}|\Psi_g\rangle=\langle rs|D_z|\Psi_g\rangle+\sum_{t,u}\frac{\langle rs|1/r_{12}-u_1-u_2|tu\rangle\langle tu|D_{\rm eff}|\Psi_g\rangle}{E_0+\omega-\varepsilon_t-\varepsilon_u+i\eta}\ . \tag{7}$$

Before the dipole interaction we effectively sum over all intermediate states by the use of a nearly exact ground-state wave function using the pair equation. After the dipole interaction rs and tu are restricted to belong to the nine final-state channels which are included. The unknown effective-dipole-matrix elements from the ground state to a basis function in the included final-state channels, represented by the diagram on the left-hand side of the equation in Fig. 2, depend on all the unknown effective-dipole-matrix elements through the last three terms on the right-hand side (rhs). This equation could be solved iteratively by first neglecting the last three terms to get lowest-order dipole-matrix elements, which then can be used to calculate approximate corrections to the right-hand side from the last three terms of the equation which is solved again, and so on to self-consistency. Convergence problems occur close to resonances and we prefer to invert the matrix for the unknown effective-dipole-matrix elements by Gaussian elimination.

In each of the nine channels we have eight bound and 42 continuum states, giving us 450 unknown complex effective-dipole-matrix elements $\langle rs|D_{\rm eff}|\Psi_g\rangle$. Due to the ω dependence in the denominator of the last term in Eq. (7) the 450×450 matrix has to be constructed for each ω value considered, while the dipole-matrix elements $\langle rs|D_z|\Psi_g\rangle$ and the Coulomb matrix elements $\langle rs|1/r_{12}-u_1-u_2|tu\rangle$ can be calculated once and for all and read in. The coupled equations denoted by Fig. 2 can be written so that the unperturbed dipole-matrix elements occur as a driving term in the equations, and solution for the length and velocity forms of the dipole operator can thus be done simultaneously.

In the coupled integral equations [Eq. (7)] t, say, is a bound He^+ orbital and u is summed over excited bound states and integrated over continuum states. The summation over the bound states beyond the eight explicitly included and the continuum integration from the origin to the lowest continuum mesh point, has been included by using the fact that the scaled matrix elements are continuous over the ionization limit, e.g.,

$$\lim_{n\to\infty}\langle t,nl|D_{\rm eff}|\Psi_0\rangle(n^*)^{3/2}=\lim_{k\to 0}\langle t,kl|D_{\rm eff}|\Psi_0\rangle\sqrt{2/\pi k}\ , \tag{8}$$

and using linear interpolation between the last bound and

the first continuum state to estimate the matrix elements in that region. Here $n^*=n-\delta$ is the effective quantum number, where δ is the quantum defect which is extrapolated from the two highest bound states, and k is the wave vector related to the energy by $E=\frac{1}{2}k^2$. The summation (integration) from the last bound state to the first continuum state thus affects the coefficients in front of the unknown effective-dipole-matrix elements involving the highest bound and first continuum orbital, in the system of integral equations. In deriving Eq. (8) we have made use of Eq. (3) describing the normalization of our continuum functions.

Some care has to be taken when integrating over a pole in Eq. (7). The numerator consists of a Coulomb and an effective-dipole-matrix element. Both are assumed to vary smoothly over the pole as a function of the wave vector k of the continuum orbital t or u. For the effective-dipole-matrix element this is assumed for a fixed value of ω while, of course, this matrix element varies rapidly as a function of ω over a resonance. By assuming a four-point Lagrange expansion of the numerator, we can integrate analytically each power of k over the pole giving contributions to the coefficients in the coupled integral equations.

One way to take into account the effects of the higher-excited channels in an approximate way is to include channels based on "pseudo-states," modified orbitals chosen to have a large overlap with the final-state ionic orbitals which was done, e.g., by Berrington *et al.*[14] Another way would be to calculate perturbatively to lowest order the corrections to the Coulomb matrix elements coupling the included channels, due to the interaction with the neglected channels. One example of a correction to the interaction between the $2skp$ and $2pkd$ channels coming from the influence of higher-excited $k'pk''d$ channels is

$$\langle 2pk_2d|r_</r_>^2|2sk_1p\rangle_{\text{correction}}=\sum_{k',k''}\frac{\langle 2pk_2d|r_<^2/r_>^3|k'pk''d\rangle\langle k'pk''d|r_</r_>^2|2sk_1p\rangle}{E_0+\omega-\varepsilon_{k'}-\varepsilon_{k''}+i\eta}A\ , \tag{9}$$

where A denotes a factor coming from the angular integration. For practical reasons one has to restrict the summation over k' and k'' due to the high number of Coulomb matrix elements involved. For the intermediate higher-excited channels including double continuum channels, one continuum orbital could be calculated using a V^{N-1} potential and the other orbital by a V^{N-2} potential,[36] thus approximately cancelling higher-order effects within the higher-excited channels. This choice of potential gave good agreement with experiment for the double photoionization of helium.[44]

C. Resonances

When the energy denominator in Eq. (7) vanishes for a discrete intermediate configuration tu, degenerate with the final continuum rs, a resonance occurs in the corresponding continuum channel. For example, below the threshold for photoionization with excitation to $2s$ and $2p$ levels of He^+ (the $n=2$ threshold) three series of resonances due to doubly excited states occur in the $1s$ cross section. The designations $2sn'p$, $2pn's$, and $2pn'd$ for these series are not appropriate, as first pointed out by Cooper, Fano, and Prats.[45] They introduced the + and − series $2sn'p+2pn's$ and $2sn'p-2pn's$ to explain why only a single series (+) was observed in the early observations by Madden and Codling.[27]

It is probably fair to say that most of the accurate calculations of energies and widths for doubly excited states still come from configuration-interaction-type methods. Other approaches may, however, give a much better physical understanding of the nature of these states. The use of hyperspherical coordinates was introduced by Macek[46] and has been developed further by, e.g., Lin.[47] The systematics of doubly excited states has also been interpreted in terms of a molecularlike rotation and vibration model.[48,49] A comparison between such collective motion and the independent-particle motion has been made by Ezra and Berry.[50]

Herrick and Sinanoğlu,[21] by group-theoretical methods, derived expressions for linear combinations of the $nln'l'$ series that approximately diagonalize the Coulomb interaction. These were denoted by new quantum numbers K and T. Here n is the principal quantum number for the inner electron and n' the same for the outer electron. For the ^1P resonances, relevant for he photoionization from the ground state of He, only K needs to be specified and can take on the values $K=\pm n,\pm(n-1),\ldots,0$. For the resonances below the $n=2$ threshold with $n=2$ the + series corresponds approximately to $K=0$, the − series to $K=+1$ and the $2pn'd$ to $K=-1$. Herrick and Sinanoğlu were also able to predict selection rules that certain K series are approximately forbidden to autoionize.[21] Thus the $K=-1$ series below the $n=2$ threshold is forbidden, giving rise to very sharp resonances not possible to resolve with the present experimental energy resolution. We shall denote the resonances by $K_{n'}$ for a particular n.

For an isolated autoionizing state interacting with a single continuum the cross-section resonance profile is given by the Fano formula,[51]

$$\sigma=(\sigma_0+\varepsilon\sigma_1)\frac{(\varepsilon+q)^2}{1+\varepsilon^2}\ , \tag{10}$$

where ε is the normalized energy distance to the resonance energy E_r,

$$\varepsilon=\frac{E-E_r}{\Gamma/2} \ . \tag{11}$$

Here Γ is the width of the resonance and q the line-shape parameter.[51] The background cross section at the resonance is σ_0 and we have also allowed for a slope in the background cross section by introducing $\varepsilon\sigma_1$. Neglecting the background factor, the resonance has a maximum of $1+q^2$ at $\varepsilon_{\max}=1/q$ and is zero at $\varepsilon_{\min}=-q$. The sign of q thus determines whether the maximum occurs before or after the minimum, and the magnitude of q indicates the excess over the background cross section. If $q=0$ there is no maximum and we get a window resonance.

If there are several continua interacting with the autoionizing state, the Fano formula above has to be modified. Then the cross section does not go to zero and one has to introduce a correlation index ρ^2 that tells how much the background cross section is depleted at minimum[52]

$$\sigma=(\sigma_0+\varepsilon\sigma_1)\left[(1-\rho^2)+\rho^2\frac{(\varepsilon+q)^2}{1+\varepsilon^2}\right] \ . \tag{12}$$

This formula has been used to examine the three sharp series of resonances below the $n=3$ threshold.

D. Angular distribution

The angular asymmetry parameter $\beta(\omega)$ is defined through the equation

$$\frac{d\sigma(\omega)}{d\Omega}=\frac{\sigma(\omega)}{4\pi}\{1+\beta(\omega)[3\cos^2(\theta)-1]/2\} \ , \tag{13}$$

where θ is the angle between the electric vector of the incident radiation and the momentum of the ejected photoelectron. Since the differential cross section is a positive quantity the range for β is from -1 to 2. General formulas for $\beta(\omega)$ have been derived by Lipsky,[53] Jacobs,[54] and by Dill and Fano.[55] In many cases these general formulas reduce to the central-field formula derived by Cooper and Zare[56] and generalized to allow for complex-dipole-matrix elements by Amusia *et al.*[57] (Note that there is a sign error in the latter reference which has been corrected in a later review article.[33]) This formula, which is applicable in this work since the angular momentum L_0 of the initial state is zero, reads

$$\beta=\frac{l(l-1)|R_{l-1}|^2+(l+1)(l+2)|R_{l+1}|^2-6l(l+1)\,\mathrm{Re}(\chi)}{(2l+1)[l|R_{l-1}|^2+(l+1)|R_{l+1}|^2]} \ , \tag{14}$$

where in our case $l=L_b$ is the angular momentum of the ion left behind. R_{l-1} and R_{l+1} are defined through the reduced matrix element of the dipole operator as

$$\langle L_bS_bl_1s_1L_1S_0||D||L_0S_0\rangle=\begin{cases}-\sqrt{l}\,R_{l-1} & \text{if } l_1=l-1\\ \sqrt{(l+1)}R_{l+1} & \text{if } l_1=l+1 \ ,\end{cases} \tag{15}$$

and χ is

$$\chi=R^*_{l-1}R_{l+1}\exp[i(\sigma_{l+1}+\delta_{l+1}-\sigma_{l-1}-\delta_{l-1})] \ . \tag{16}$$

Here l_1 refers to the angular momentum of the photoelectron and L_1 to the total angular momentum of the final state. Including final-state correlation gives imaginary contributions to the reduced-dipole-matrix elements. Through Eq. (16) this can be interpreted as an extra phase shift δ_{corr} not included in the basis functions

$$\langle L_bS_bl_1s_1L_1S_0||D||L_0S_0\rangle = \exp(i\delta_{\mathrm{corr}})|\langle L_bS_bl_1s_1L_1S_0||D||L_0S_0\rangle| \ . \tag{17}$$

If also $L_b=l=0$, only the second term contributes in Eq. (14) and β is exactly 2.

If we do not distinguish between some ionic states, the total angular asymmetry parameter β_{tot} is the weighted average of β_b for the different ionic states

$$\beta_{\mathrm{tot}}=\sum_b\beta_b\sigma_b\Big/\sum_b\sigma_b \ , \tag{18}$$

where σ_b is the partial cross section for leaving the ion in the state b.

III. NUMERICAL CONSIDERATIONS

A. Sharp peaking of Coulomb matrix elements

When calculating the Coulomb matrix elements, care has to be taken to integrate far enough out if a coordinate involves two continuum or highly excited bound orbitals. For the monopole matrix element of the type $\langle 2skp|1/r_>|3sk'p\rangle$, there is no problem, since the contribution, when the second integration variable is greater

than the range of the $2s$ and $3s$ orbitals, is zero due to the orthogonality of the $2s$ and $3s$ orbitals involved in the first integration variable. The worst case occurs for dipole-matrix elements of the type $\langle 2skp|r_<^2/r_>^2|2pk's\rangle$. Here we have tail corrections from the integration over the second coordinate that go as one over the cutoff radius for this integration. These become significant when k' is close to k. Care was taken to integrate very far out in this case. The resulting matrix elements were found to peak sharply around $k'=k$ as a function of k' and seem to have a cusp at $k'=k$.

The sharp peaking discussed above is particularly troublesome for the system considered here due to the degeneracy of the $2s$ and $2p$ ionic states. This implies that the numerator in the last term of Eq. (7) peaks sharply and has a cusp exactly where we have a pole in the integration. An oscillatory behavior as a function of ω was observed for the cross sections between points corresponding to the k mesh used. This behavior was to a large extent eliminated by interpolating the calculated matrix elements to a new k mesh with one point corresponding exactly to the wanted ω value. This new k mesh was then used in the coupled-equation code. An asymmetric Lagrange interpolation formula was used on each side of the cusp.

B. Blocking technique

As mentioned in Sec. II, when using the coupled-integral-equation technique, we have to set up and solve a system of linear equations for our 450 unknown complex-effective-dipole-matrix elements. This has to be done for each ω value considered. Due to the limited core memory we could not store the whole matrix simultaneously and a blocking technique was used. The 450 unknowns originate from nine channels with 50 basis states (eight bound and 42 continuum) in each channel. This gives rise to a natural block structure of our matrix where the coefficients originating from a particular channel in front of the unknowns corresponding to another channel occur as a 50×50 block and the full matrix thus has 9×9 blocks. This 9×9-block matrix equation was solved by Gaussian elimination, formally treating each block as a number and only having a few relevant blocks in the core memory at a time.

The technique discussed above works very well numerically. The CPU time for solving our 450×450 complex matrix equation is about 90 sec on the CDC-Cyber 855 used and the real time about twice that if there is no competition with other users. As mentioned, this is done simultaneously for the length and velocity forms of the dipole operator without any significant extra CPU time. In addition to the time spent for each desired ω, however, we have spent time to calculate the basis states used and all the Coulomb and first-order dipole-matrix elements.

C. A test of the coupled-equation code

In Sec. II we defined the orbitals used to represent the channels included in the final state. The p orbitals were generated in the ^1P potential of a $2s$ He^+ orbital with projection operators to assure orthogonality to the $2p$ and $3p$ He^+ orbitals used. This choice is a good one to represent the $2skp$ channel and was chosen since the emphasis in this work is on photoionization with excitation to the $n=2$ states. For the main channel $1skp$, however, the p orbitals used are rather unphysical. The natural choice for this channel would, of course, be a ^1P potential with a $1s$ He^+ orbital. With this choice of potential there is no further final-state correlation within the $1skp$ channel.[58]

Since the p orbitals in the $2s$ potential that we use form a complete set, we should be able to reproduce the results obtained with the $1s$ potential, if we include final-state correlation to all orders within the $1skp$ channel. This can be done with our coupled-equation code and can be used as a test of the numerical accuracy of the code. In Table I the first two columns show the length and velocity results for the $1skp$ cross section using our almost exact ground-state wave function and p orbitals in the $2s$ potential for the final state with no final-state correlation included. The results are rather poor as can be see by comparison with similar results using p orbitals in the $1s$ potential in the last two columns. The middle two columns show the results when the coupled-equation code has been used to correct the first two columns by including all final-state correlations within the $1skp$ channel. The agreement between the middle and the last two columns is rather good, which gives us confidence in our coupled-equation code and shows that the orbitals we use do not introduce any significant error via a possibly poorly represented $1skp$ channel.

IV. RESULTS

A. Resonances below the $n=2$ threshold

As mentioned in the Introduction, the first observation of doubly excited states in total photoabsorption was made by Madden and Codling[27,26] using synchrotron radiation. Their resolution was also good enough to study the line profiles for the broadest resonances. In their later work both the + and − series discussed in the theory section were observed.

Early calculations of the resonances below the $n=2$ photoionization threshold at 65.4 eV were made by Burke, McVicar, and Smith,[59] by Burke and McVicar[60] using the close-coupling approximation, by O'Malley and Geltman[61] applying the Feshbach projection-operator formalism, and by Altick and Moore[62] and Lipsky and Russek[63] using diagonalization methods. Subsequently these resonances have been studied extensively by different theoretical methods. Bhatia and Temkin[64] applied the Feshbach projection-operator formalism. Burke and Taylor[65] included extra short-range correlation terms in the close-coupling approximation. Balashov *et al.*,[66] Herrick and Sinanoğlu,[21] Lipsky and Coneely,[67] and Lipsky *et al.*[68] have used diagonalization methods. Macek[46] introduced hyperspherical coordinates. Doyle *et al.*[69] used a bound-state expansion method. Drake and Dal-

TABLE I. The $1skp\ ^1P$ cross section in Mb calculated in the one-channel approximation with various methods, in order to test the accuracy of the coupled-equation code.

	kp in $2s$ potential[a]		Coupled equations[b]		kp in $1s$ potential[c]	
k (a.u.)	Length	Velocity	Length	Velocity	Length	Velocity
0.05	0.3923	1.3890	7.2361	7.0794	7.2359	7.0798
0.1	0.4030	1.4226	7.1948	7.0383	7.1947	7.0384
0.2	0.4445	1.5508	7.0312	6.8741	7.0317	6.8748
0.4	0.5874	1.9685	6.4156	6.2574	6.4137	6.2561
0.6	0.7407	2.3657	5.5089	5.3537	5.5077	5.3524
0.8	0.8049	2.4608	4.4781	4.3315	4.4780	4.3316
1.0	0.7400	2.1892	3.4828	3.3503	3.4840	3.3510

[a] kp states calculated in $2skp\ ^1P$ potential.
[b] Coupled-equation code used to correct for use of $2skp\ ^1P$ potential in calculating basis states. Only $1skp\ ^1P$ channel included.
[c] kp states calculated in $1skp\ ^1P$ potential. Note close agreement with coupled-equation result using $2skp\ ^1P$ basis states.

garno[70] made a $1/Z$ expansion. Chung and Chen[71] used a projection-operator formalism. The complex coordinate method was used by Hickman *et al.*,[72] Ho,[73] and by Chung and Davis.[74] McGreevy and Stewart[75] applied perturbation theory for the phase shift. Berrington *et al.*[14] used the close-coupling approximation with pseudostates. The multichannel quantum-defect theory was used by Ohja[76] and Oza[77] used an algebraic variational method. Particularly the $2s2p$ resonance has been studied carefully, stimulating a remeasurement of the position, width, and line-shape parameter for this resonance by Morgan and Ederer.[78]

Since the $n=2$ channels are included in our work, all three series of resonances in the $1s$ channel below the $n=2$ threshold show up in our calculation of the cross section. A fit of the cross section to the Fano formula Eq. (10) was made for each resonance and the parameters describing the resonance were determined. The results are presented in Table II. The total nonrelativistic energy for the ground state is 2.903 724 a.u. (Refs. 79 and 29). Transforming the calculated energies to electron volts we have used the reduced Rydberg constant 13.603 975. This gives the double-ionization limit 79.0044 eV. No mass-polarization (specific-mass shift) effects and no relativistic or Lamb-shift effects are included.

We will not compare our results with all previous calculations and have chosen to compare with the four-channel close-coupling calculation of Burke and McVicar[60] and with the recent accurate calculation of positions and widths by Oza[77] using an algebraic variational method. The latter calculation is within the error bars of the latest experimental results. We present two sets of results. The first set only includes four channels, the main channel and the three $n=2$ channels. The second set in addition includes the five $n=3$ channels. As can be seen from the results presented in Table II our four-channel calculation is almost identical to the close-coupling calculation by Burke and McVicar. By comparing our nine-channel calculation with the accurate results by Oza, we can see a marked improvement over the four-channel calculation by including the $n=3$ channels. Our calculation is not a state-of-the-art one for the $2s2p$ resonance, but the agreement with the accurate results by Oza improves rapidly going to higher-excited resonances. Note that the $1_{n'+1}$ and $-1_{n'}$ resonances are almost degenerate and that their relative position changes between the four-channel and nine-channel calculations. This affects the widths and line-shape parameters drastically and we conclude that inclusion of higher-excited channels is essential to get the width and line shape of these resonances accurately.

B. The $n=2$ channels

In this section we present the $n=2$ cross sections and angular asymmetry parameters from threshold at 65.4 eV to 130 eV. Since no channels based on $n \geq 4$ He^+ states are included in the present calculation we are missing all resonance structure above the $n=3$ threshold at 73.0 eV up to the double-ionization threshold at 79.0 eV. Comparison with experiment in this region is unreliable. Our results should be less accurate in the higher-energy region due to the neglect of the higher-excited channels. This also shows up in worse agreement between our length and velocity results at higher energies.

The only experiment so far that directly separates the $2s$ and $2p$ cross sections was performed by Woodruff and Samson.[9,10] They monitored the 304-Å fluorescence light with and without an applied electric field that caused mixing between the $2s$ and $2p$ levels. In Figs. 3 and 4 we compare our results for the $2s$ and $2p$ cross sections with their data. We also present the results of the close-coupling calculation by Jacobs and Burke.[12] Our four-channel calculation gives results very close to the results by Jacobs and Burke, and a comparison with our nine-channel calculation presented in the figures thus gives the effect of the $n=3$ channels.

The total $n=2$ $(2s+2p)$ cross section is presented in Fig. 5 together with previous experimental determinations.[8,10,80] We have also included the velocity calculation by Jacobs and Burke,[12] which they favor over their length calculation due to their well-correlated ground state, and the length result of Berrington *et al.*,[14] which they claim is more accurate than their velocity result. As before, the comparison with Jacobs and Burke gives the effects of including the $n=3$ channels.

In a previous paper[28] we presented the ratio σ_{2p}/σ_{2s}, which is approximately three at threshold, in agreement

TABLE II. Parameters describing the resonances in the $1skp$ cross section below the $n=2$ ionization limit. The integers in brackets denote powers of ten. The resonance energies and widths are given in eV and the σ parameters in Mb. The nonrelativistic value 79.0044 eV has been used for the double-ionization energy as discussed in the text.

Resonance[a]	Parameter	This work 4 channels	This work 9 channels	Burke and McVicar[b]	Oza[c]
0_2	E_0	60.266	60.184	60.269	60.155
	Γ	4.37[−2]	4.03[−2]	4.38[−2]	3.61[−2]
	$q(l)$	−2.56	−2.63	−2.59	
	$q(v)$	−2.66	−2.70	−2.65	
	$\sigma(l)$	1.405	1.412	1.415	
	$\sigma(v)$	1.363	1.375	1.380	
1_3	E_0	62.770	62.759	62.773	62.759
	Γ	1.36[−4]	1.13[−4]	1.39[−4]	1.06[−4]
	$q(l)$	−3.75	−4.00	−3.02	
	$q(v)$	−3.82	−4.07	−3.75	
	$\sigma(l)$	1.275	1.281	1.280	
	$\sigma(v)$	1.235	1.247	1.247	
0_3	E_0	63.688	63.670	63.691	63.659
	Γ	8.81[−3]	8.96[−3]	8.72[−3]	8.5[−3]
	$q(l)$	−2.44	−2.43	−2.44	
	$q(v)$	−2.52	−2.50	−2.51	
	$\sigma(l)$	1.246	1.249	1.250	
	$\sigma(v)$	1.207	1.215	1.218	
1_4	E_0	64.132	64.140	64.134	64.136
	Γ	4.92[−5]	6.84[−5]	5.03[−5]	5.66[−5]
	$q(l)$	−3.75	−2.32	−3.02	
	$q(v)$	−3.82	−2.48	−3.75	
	$\sigma(l)$	1.275	1.208	1.280	
	$\sigma(v)$	1.235	1.175	1.247	
-1_3	E_0	64.171	64.125	64.172	
	Γ	2.26[−6]	3.30[−6]	1.54[−6]	
	$q(l)$	0.969	−4.00	−0.10	
	$q(v)$	0.796	−4.07	+0.92	
	$\sigma(l)$	1.207	1.281	1.213	
	$\sigma(v)$	1.168	1.247	1.179	
0_4	E_0	64.479	64.471	64.481	64.466
	Γ	3.68[−3]	3.84[−3]	3.69[−3]	3.77[−3]
	$q(l)$	−2.42	−2.41	−2.42	
	$q(v)$	−2.49	−2.47	−2.49	
	$\sigma(l)$	1.249	1.211	1.214	
	$\sigma(v)$	1.171	1.179	1.183	
1_5	E_0	64.656	64.660	64.658	64.658
	Γ	2.27[−5]	3.34[−5]	2.30[−5]	2.77[−5]
	$q(l)$	−4.04	−2.28	−3.42	
	$q(v)$	−4.11	−2.44	−4.04	
	$\sigma(l)$	1.177	1.182	1.182	
	$\sigma(v)$	1.139	1.149	1.150	
-1_4	E_0	64.674	64.652	64.676	
	Γ	1.17[−6]	9.67[−7]	7.76[−7]	
	$q(l)$	1.44	−12.91	0.66	
	$q(v)$	1.21	−12.49	1.50	
	$\sigma(l)$	1.182	1.191	1.188	
	$\sigma(v)$	1.144	1.158	1.155	

TABLE II. (*Continued*).

Resonance[a]	Parameter	This work 4 channels	This work 9 channels	Burke and McVicar[b]	Oza[c]
0_5	E_0	64.823	64.818	64.824	64.816
	Γ	1.89[−3]	1.97[−3]	1.89[−3]	1.79[−3]
	$q(l)$	−2.41	−2.40	−2.41	
	$q(v)$	−2.49	−2.46	−2.48	
	$\sigma(l)$	1.194	1.194	1.198	
	$\sigma(v)$	1.156	1.162	1.167	
0_6	E_0	65.004	65.001		65.000
	Γ	1.09[−3]	1.04[−3]		1.0[−3]
	$q(l)$	−2.40	−2.39		
	$q(v)$	−2.48	−2.46		
	$\sigma(l)$	1.185	1.185		
	$\sigma(v)$	1.147	1.153		
0_7	E_0	65.112	65.110		65.110
	Γ	6.85[−4]	7.17[−4]		
	$q(l)$	−2.40	−2.39		
	$q(v)$	−2.48	−2.46		
	$\sigma(l)$	1.180	1.180		
	$\sigma(v)$	1.142	1.147		

[a] Notation from Herrick and Sinanoğlu (Ref. 21).
[b] Burke and McVicar (Ref. 60).
[c] Oza (Ref. 77).

with recent experiments[6,8,10] and calculations by Jacobs and Burke[12] and Berrington *et al.*[14] but in disagreement with the calculation by Chang.[13]

The ratio ξ between the $2pkd$ cross section and the total $2p$ cross section is of importance in describing helium photoionization with excitation to the $2p$ state.[16] In Fig. 6 we present our results for this parameter and compare with results from Scott and Burke.[16] Close to threshold our length and velocity curves are very close and agree with the length result of Scott and Burke. At higher energies the length result of Scott and Burke, which they claim is the more accurate one, is much lower than their velocity results. Our curves at higher energies are closer to their velocity result. As mentioned, however, our curves at higher energies could be affected appreciably by the neglected higher-excited channels. These are included in an approximate way in the work by Scott and Burke by including channels based on pseudostates.

Recently Jiménez-Mier *et al.*[81] have measured the angular distribution of the 304-Å fluorescence light from the ion following the photoionization with excitation to $n=2$ states. This was done at two energies close to the $n=2$ photoionization threshold. From this angular dis-

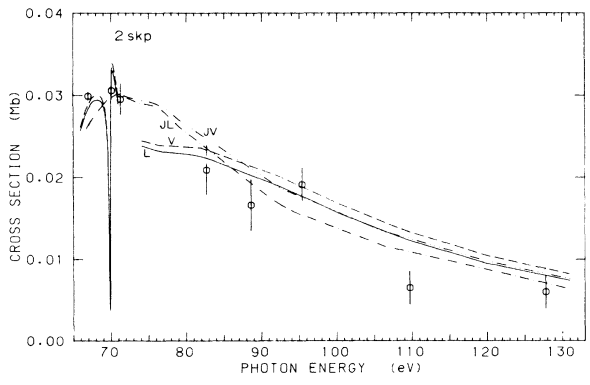

FIG. 3. The $2s$ partial cross section. Present calculation in the length (L, ——) and velocity (V, — — —) forms of the dipole operator are compared with the results of Jacobs and Burke (Ref. 12) in the length (JL, —·—·—) and velocity (JV, — · · · —) forms. The open circles with vertical lines represent experimental data and error bars from Woodruff and Samson (Ref. 10).

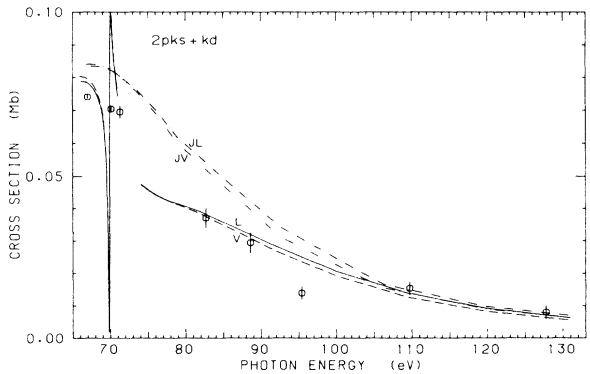

FIG. 4. The $2p$ ($2pks+2pkd$) partial cross section. The same notation as in Fig. 3.

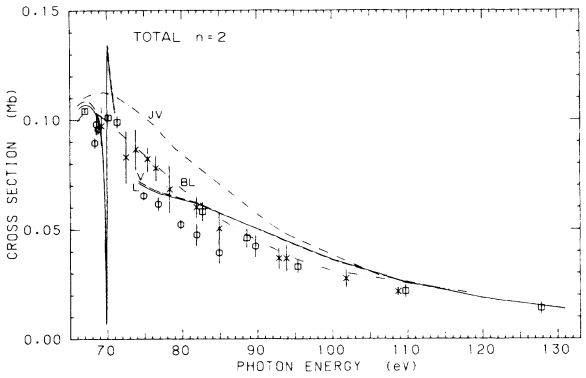

FIG. 5. The total $n=2$ cross section (the sum of the $2s$ and $2p$ cross sections). Present calculations in the length (L, ——) and velocity (V, — — —) forms are compared with the length result (BL, – · · · –) of Berrington *et al.* (Ref. 14) and with the velocity result (JV, –·–·–) of Jacobs and Burke (Ref. 12). The different symbols with vertical lines represent experimental data with error bars. ×, Wuilleumier *et al.* (Ref. 80); □, Woodruff and Samson (Ref. 10); ○, derived from Lindle *et al.* (Ref. 8) using our velocity results for the $1s$ cross section.

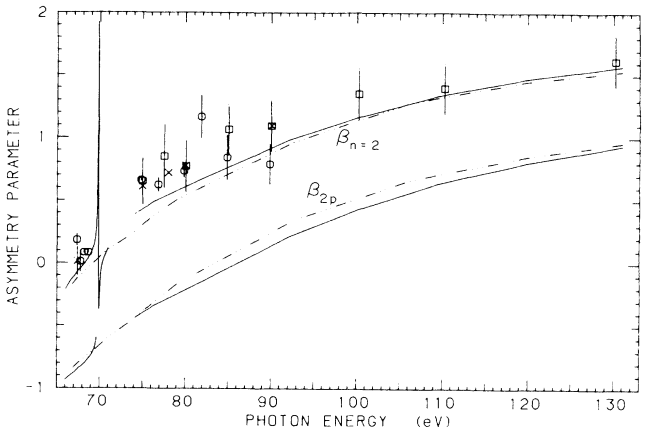

FIG. 7. The asymmetry parameter for the $2p$ cross section (the two lower curves) and for the total $n=2$ cross section (the two upper curves and the experimental data points). Present calculation in the velocity form (——) is compared with the calculation of Jacobs and Burke (Ref. 12) in the velocity form (– · · · –). The different symbols with vertical lines represent experimental results with error bars. □, Bizau *et al.* (Ref. 5); ×, Schmidt *et al.* (Ref. 6); ○, Lindle *et al.* (Ref. 8).

tribution they were able to determine the ξ parameter discussed above and the closely related alignment of the resulting He^+ ion[82] that depends linearly on the ξ parameter. Their results for ξ, 0.25±0.04 at photon energy 65.5 eV and 0.25±0.03 at 66.4 eV, are in agreement with our calculation that gives 0.248 and 0.266, respectively, at these energies. This gives confidence in our calculation close to the $n=2$ threshold. Scott and Burke[16] do not present any results for ξ below 69 eV, but their results at 69 eV are essentially in agreement with ours, with only 10% difference between their length and velocity results.

In Fig. 7 we present our velocity result for the asymmetry parameter β, both for the $2p$ and for the total $n=2$ cross section. (Our length and velocity results are close.) For β_{2p} we have used the generalized Cooper and Zare formula, Eq. (14). The phase shifts $\delta_{l\pm1}$ were calculated from our continuum functions using a WKB method. Complex-dipole-matrix elements from our coupled-equation code were used; these matrix elements include the correlation contribution to the phase shifts. For $\beta_{n=2}$ we have used Eq. (18) to average over β_{2s} and β_{2p}. As discussed in Sec. II D, $\beta_{2s}=2$ since here both the initial state and the final ionic state have $L=0$. In the figure we also give the velocity results of Jacobs and Burke[12] for comparison. Their results are close to ours, indicating that the inclusion of the $n=3$ channels is not so important for this parameter. Several experimental results of the asymmetry parameter for the total $n=2$ cross section are also included in the figure. There is a tendency for the experimental points to be higher than the theoretical curves.

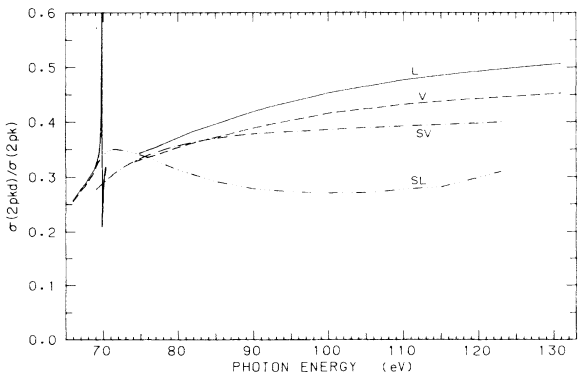

FIG. 6. The ratio ξ between the $2pkd$ cross section and the $2p$ ($2pks+2pkd$) cross section. Present calculation in the length (L, ——) and velocity (V, — — —) forms are compared with the results of Scott and Burke (Ref. 16) in the length (SL, – · · · –) and velocity (SV, –·–·–) forms.

C. Resonance region below the $n=3$ threshold

Below the $n=3$ threshold at 73.0 eV there is resonance structure in the $1s$ and the $n=2$ channels due to doubly excited states with one electron in an $n=3$ state. In LS coupling one would expect to see five different series of autoionizing resonances due to the five channels $3skp$, $3pks$, $3pkd$, $3dkp$, and $3dkf$. As discussed in the theory section, Herrick and Sinanoğlu[21] found that other linear combinations of these channels, denoted by a new quantum number $K=\pm2$, ±1, or 0, approximately diagonalize the Coulomb interaction among the five channels. The resonances are thus denoted by $K_{n'}$, where n' is the prin-

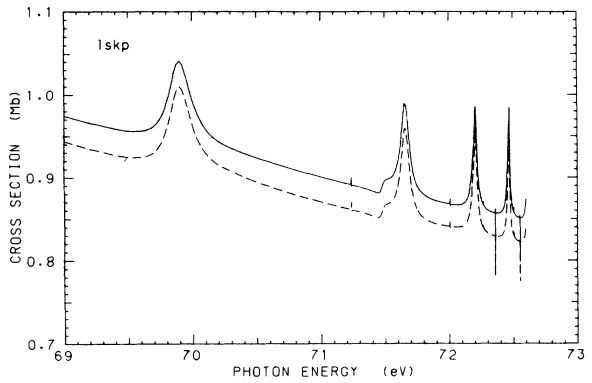

FIG. 8. The 1*skp* partial cross section in the resonance region leading up to the $n=3$ threshold at 73.0 eV. The solid (dashed) curve represents the present calculation using the length (velocity) form of the dipole operator. Note that the cross-section scale does not start from zero.

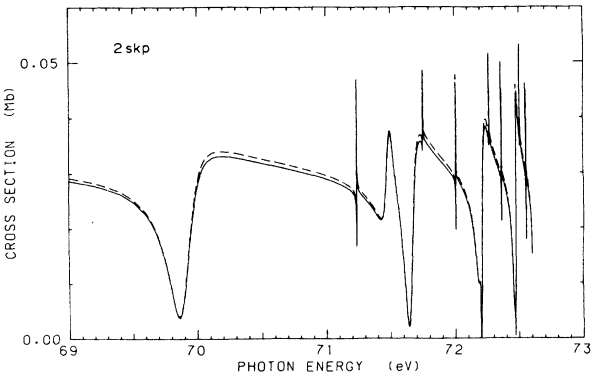

FIG. 9. The 2*skp* partial cross section. The same notation as in Fig. 8.

cipal quantum number of the outer electron. We note that our coupled-equation approach diagonalizes the Coulomb interaction among all included channels and therefore produces the appropriate linear combinations. Herrick and Sinanoğlu were also able to predict selection rules that the three series with $K=\pm 2,0$ are approximately forbidden to autoionize, giving rise to very sharp resonances not possible to detect with the present experimental resolution.

Several states in the stronger of the two allowed series with $K=+1$ were observed by Madden and Codling[26] in total photoabsorption. The width and line profile in total photoabsorption of the first resonance in this series were measured by Dhez and Ederer.[83] Later, Woodruff and Samson[9,10] found that the resonance structure was much more pronounced in the $n=2$ partial cross sections where they also found indications of the first resonance in the weaker allowed series with $K=-1$. Their findings were later confirmed by Lindle and co-workers,[7,8] who also measured the $n=2$ angular asymmetry parameter β in the resonance region.

In Figs. 8–13 we present the various partial cross sections for the open channels in the resonance region below the $n=3$ threshold. Note that in Figs. 8 and 13 the cross-section scale does not start from zero, which might give a false impression of the strength of the resonance structure and the agreement between the length and velocity results. From the figures we clearly see that the relative strength of the resonance structure is much more pronounced in the partial $n=2$ cross sections than in the 1*skp* or total cross sections. The absolute strength, though, is of the same order. Another interesting observation is the different line shapes and strengths of the resonances in the different partial cross sections.

In our previous paper[28] we presented the total $n=2$ cross section and obtained good agreement with experimental results by Woodruff and Samson[10] and by Lindle *et al.*[8] although the calculated results are a little higher

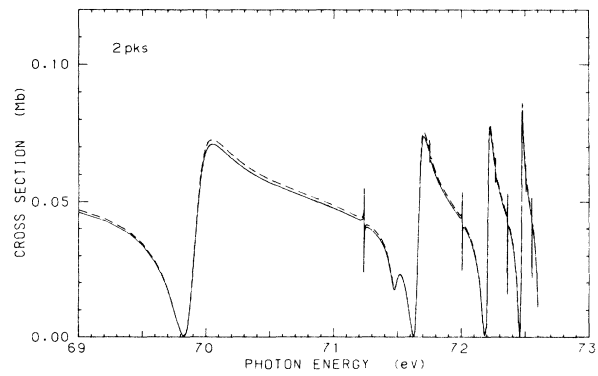

FIG. 10. The 2*pks* partial cross section. The same notation as in Fig. 8.

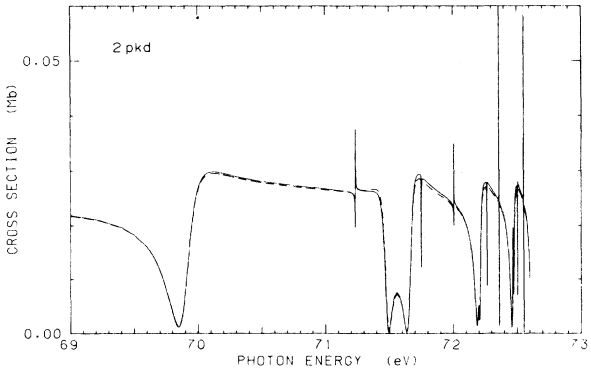

FIG. 11. The 2*pkd* partial cross section. The same notation as in Fig. 8.

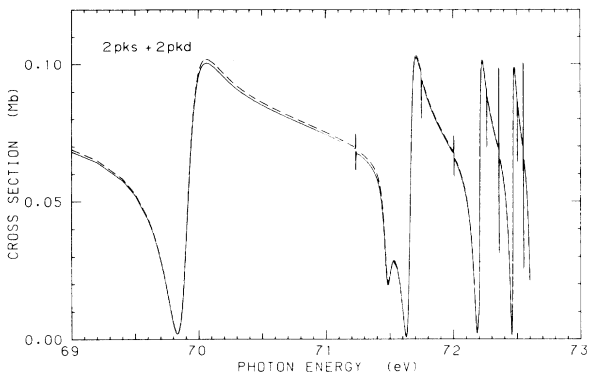

FIG. 12. The $2p$ ($2pks+2pkd$) partial cross section. The same notation as in Fig. 8.

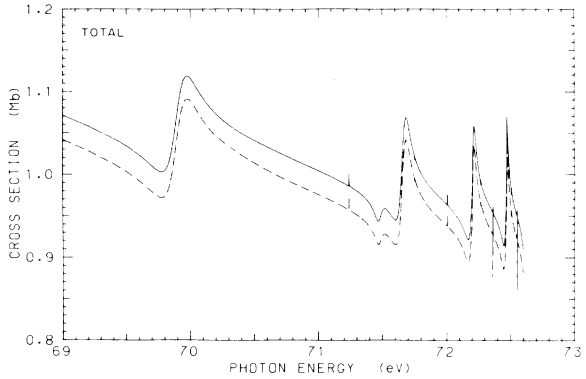

FIG. 13. The total cross section ($1s+2s+2p$). The same notation as in Fig. 8. Note that the cross-section scale does not start from zero.

than experiment, particularly than the results of Woodruff and Samson.

The first resonance of the weaker of the two allowed series occurs in our calculation at about 71.4 eV while the remaining ones are overpowered in the stronger series. Our calculation also reveals the three sharp series although not all of them are resolved in the scale of the figures.

Several theoretical calculations of the resonances below the $n=3$ threshold exist. Ormonde *et al.*[17] used the close-coupling method for the first $K=1$ resonance and the same method was used by Burke and Taylor[18] also including short-range correlation. Oberoi[19] and Chung[20] calculated the energy positions of resonances in all K series using the Feshbach projection-operator formalism. Herrick and Sinanoğlu[21] also calculated positions of resonances in all K series, using configuration interaction of bound states, and corresponding widths using screened Coulomb continuum functions. Senashenko and Wagué[22] used the diagonalization method of Balashov *et al.* on the four resonances lowest in energy. Ho[23,24] has used the complex rotation method to calculate the positions and widths of some of the lowest resonances.

For the three sharp series we made fits of the resonances in the total $n=2$ cross section to the Fano formula [Eq. (12)] with several open channels. In Table III we compare our results with previous theoretical calculations for the sharp resonances. We observe the near degeneracy of the $-2_{n'}$ and $2_{n'+2}$ resonances. In analogy with the degenerate resonances below the $n=2$ threshold we might expect the widths and shapes of these resonances to be sensitive to their relative positions and thus to the inclusion of higher-excited channels.

For the energy positions the differences between the calculations are small. The calculated widths, however, differ considerably between the different calculations. For the $K=2$ series ours are about a factor 1.7 larger than the ones reported in Refs. 21 and 22. Both these calculations use configuration interaction among bound states in the five $3ln'l'$ channels, included in our work, to describe the autoionizing states. The widths are then obtained by first-order perturbation with the continuum channels, thus neglecting continuum-channel coupling. The results in parentheses from Senashenko and Wagué[22] include the seven configurations based on unscreened He^+ orbitals with $n'\leq 4$ while their other results have $n'\leq 5$. In the work by Herrick and Sinanoğlu[21] all configurations with $n'\leq 7$ are included. We clearly see that these results converge to values different from ours. In our work we have included a complete set of states in each channel, both bound and continuum states, where the states with $n'\geq 4$ differ from the ones previously used since they are screened by a $n=2$ electron. Our calculation also includes continuum-channel coupling to all orders. The width for the 2_4 resonance calculated by Ho,[24] using the complex coordinate rotation method, is closer to our calculated width, while the width for 0_4, only given to one digit, differs considerably.

The $n=2$ angular asymmetry parameter has been measured in the resonance region by Lindle *et al.*[8] In Fig. 14 we compare our calculated curve with their data points which include a broadening contribution from the finite bandwidth of the monochromator used. Deconvolution of the instrumental broadening is not straightforward since the monochromator bandpass was on the same order of, or larger than, the widths of the resonances. In their work a deconvoluted curve, giving sharper resonances, can be found and this is reproduced in our figure. For the first resonance this deconvoluted curve agrees better with our calculation than do the direct experimental data, while their curve does not resolve separately the rest of the resonances. In the figure we also give the recent calculation of Burkov *et al.*[25]

D. The $n=3$ cross sections

Above 73.0 eV the $n=3$ channels are open. Since these channels are included in the present calculation, based on exact $n=3$ He^+ states, we also get results for the corresponding cross sections, which are presented in Table IV. These cross sections are not to be considered very accurate since no effects from higher-excited channels are included. The problem with sharp peaking of the Coulomb matrix elements, discussed in Sec. III, was also

TABLE III. Parameters describing the three sharp series of resonances in the total $n=2$ cross section below the $n=3$ ionization limit. Data values in parentheses from Ref. 22 involve fewer bound-state orbitals as explained in the text. The integers in brackets denote powers of 10. The nonrelativistic value 79.0044 eV has been used for the double-ionization energy.

Parameters	Source	2_4	0_4	2_5	0_5	-2_4 and 2_6		0_6	2_7 and -2_5	
E_0 (eV)	This work	71.230	71.745	72.000	72.259	72.3535	72.3549	72.498	72.5441	72.5461
	Chung (Ref. 20)	71.222	71.726	72.000	72.257	72.341	72.356	72.498	72.538	72.558
	Oberoi (Ref. 19)	71.222	71.721	72.000	72.251	72.326				
	Herrick and Sinanoğlu (Ref. 21)	71.230	71.744	72.006	72.259	72.353	72.359			
	Senashenko and Wagué (Ref. 22)	(71.34) 71.22								
	Ho (Ref. 24)	71.224	71.722	72.000						
Γ (eV)	This work	9.05[−4]	1.16[−3]	5.92[−4]	5.51[−4]	8.9[−5]	3.6[−4]	2.99[−4]	2.2[−4]	6.22[−5]
	Herrick and Sinanoğlu (Ref. 21)	5.60[−4]	9.27[−4]	3.42[−4]	4.12[−4]	1.11[−4]	2.12[−4]			
	Senashenko and Wagué (Ref. 22)	(1.08[−3]) 5.89[−4]								
	Ho (Ref. 24)	7.6[−4]	3[−4]	4[−4]						
$q(l)$	This work	1.66	−0.039	1.98	0.277	−0.98	2.1	0.395	3.9	−0.750
$q(v)$		1.68	−0.011	2.00	0.327	−1.12	2.2	0.448	4.0	−0.878
$\rho(l)$	This work	0.218	0.190	0.171	0.241	0.47	0.14	0.274	0.08	0.526
$\rho(v)$		0.217	0.178	0.171	0.230	0.46	0.14	0.262	0.08	0.522
$\sigma_0(l)$	This work (Mb)	0.0945	0.132	0.0952	0.125	0.096	0.095	0.123	0.098	0.0968
$\sigma_0(v)$		0.0960	0.134	0.0964	0.127	0.097	0.096	0.124	0.100	0.0980

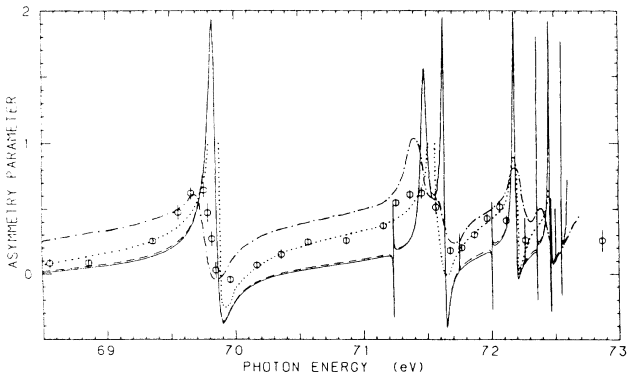

FIG. 14. The asymmetry parameter for the total $n=2$ cross section in the resonance region leading up to the $n=3$ threshold at 73.0 eV. The open circles with vertical lines represent experimental data by Lindle *et al.* (Ref. 8) with error bars. The dotted-line curve (· · · ·) is their fit to the experimental data with the monochromator broadening removed. The other curves represent theoretical calculations. Present calculation, length form (——) and velocity form (— — —) of the dipole operator; –·–·–, Burkov *et al.* (Ref. 25).

more pronounced here than for the $n=2$ cross sections. Comparison with recent experimental data by Lindle *et al.*[84] indicates that our calculated total $n=3$ cross section is about 25% too large close to the threshold at 73 eV. The experimental cross section seems to decrease monotonically with energy while our calculated one grows to a maximum at about 77 eV becoming about 80% larger than experiment in this region. In analogy with the effect on the $n=2$ cross section by including the $n=3$ channels (see Sec. IV B and Fig. 5) we can expect inclusion of the omitted higher-excited channels to reduce the $n=3$ cross section in addition to adding regions of resonance structure below the double continuum threshold at 79 eV.

Our results indicate that, among the $n=3$ channels, the $3p$ channels dominate close to the $n=3$ threshold with almost the same strength for $3pks$ and $3pkd$. In this region the $3dkp$ channel is almost as strong as the $3skp$ channel. At higher energies the $3skp$ channel becomes the dominating one while the strength in the $3dkp$ channel drops rapidly. The $3dkf$ channel is weak throughout the calculated region.

V. SUMMARY AND CONCLUSIONS

We have used many-body perturbation theory to calculate photoionization with excitation of helium. Ground-state correlation was included to all orders through the use of the pair equation.[29] Final-state correlation within the nine channels based on He^+ states with $n \leq 3$ was also included to all orders by solving a set of coupled integral equations.[30]

We have presented cross sections for the various channels with the ion excited to $2s$ and $2p$ levels. Good agreement is obtained between our length and velocity results. In regions where consistent experimental data exist, the agreement with our calculation is good. Close to threshold our calculation agrees almost exactly with the length results from Berrington *et al.*[14] and Scott and Burke.[16] At higher energies our results are closer to their velocity results while their length results for the ratios σ_{2p}/σ_{2s} and $\sigma_{2pkd}/\sigma_{2p}$ (Ref. 16) are lower than ours.

If the channels based on the $n=3$ He^+ states are ignored, we get results very close to the four-channel close-coupling calculation of Jacobs and Burke.[12] Including the $n=3$ channels we obtain the resonance structure below the $n=3$ threshold in the various $n=1$ and $n=2$ cross sections. Above the $n=3$ threshold, out to a photon energy of about 100 eV, the inclusion of the $n=3$ channels has the effect of reducing the $2s$ and $2p$ cross sections and also the ratio σ_{2p}/σ_{2s}. It is plausible that the inclusion of the neglected higher-excited channels will further reduce the ratios σ_{2p}/σ_{2s} and $\sigma_{2pkd}/\sigma_{2p}$ at higher energies. A method to include the effects of the higher-excited channels perturbatively is suggested. The angular asymmetry parameter was also calculated both in the $2p$ and the total $n=2$ cross section and was found to be less affected than the $n=2$ cross sections by the inclusion of the $n=3$ channels.

In the region below the $n=3$ threshold our calculation explains very well the resonance structure found in the experimental data for the total $n=2$ cross section by Woodruff and Samson[9,10] and by Lindle and coworkers.[7,8] The magnitudes of our cross sections, howev-

TABLE IV. Partial cross sections for photoionization with excitation to $n=3$ states in units of 10^{-3} Mb. The first column represents the photon energy and the second column the wave vector of the photoelectron. The length (velocity) results are denoted by l (v).

ω	k	$3skp$		$3pks$		$3pkd$		$3dkp$		$3dkf$		Total $n=3$		Expt.[a]
(eV)	(a.u.)	l	v	l	v	l	v	l	v	l	v	l	v	
74.19	0.3	3.86	3.90	6.98	7.05	6.18	6.18	3.01	3.12	0.58	0.65	20.6	20.9	15
76.37	0.5	4.16	4.22	8.33	8.43	7.09	7.06	2.36	2.40	0.09	0.11	22.0	22.2	13
81.67	0.8	3.41	3.52	7.81	7.99	7.33	7.19	1.50	1.36	0.23	0.18	20.3	20.3	11
92.56	1.2	2.84	3.10	3.99	4.17	3.52	3.07	0.99	0.84	0.40	0.38	11.7	11.6	7
107.8	1.6	1.97	2.28	1.77	1.83	1.56	1.16	0.34	0.28	0.24	0.22	5.86	5.78	
127.4	2.0	1.12	1.36	0.74	0.75	0.74	0.49	0.12	0.11	0.11	0.10	2.84	2.81	

[a] Interpolated from experimental data points by Lindle *et al.* (Ref. 84).

er, seem to be about 10% too high. We have also compared our calculated $n=2$ angular asymmetry parameter in this region with the experimental data of Lindle *et al.* The overall structure in the experiment was obtained in our calculation but also for this parameter there are some small deviations in magnitude.

Only the two broader series of resonances below the $n=3$ threshold are resolved with the present experimental energy resolution. In our calculation we also obtain the three sharp series of resonances. Parameters describing these sharp resonances were obtained and compared with other theoretical determinations of energy positions and widths. The energy positions agree well between the different calculations but the widths differ considerably.

Also parameters describing the resonances in the main channel below the $n=2$ threshold were obtained. The effect on these resonances from the inclusion of the $n=3$ channels was demonstrated. For the energy position one clearly sees a marked improvement including the $n=3$ channels, and except for the very lowest resonances we compare well with state-of-the-art calculations of these resonances. For the widths the situation is not that clear. We find that the resonances in the almost degenerate $1_{n'+1}$ and $-1_{n'}$ series change their relative positions when we include the $n=3$ channels. This has a strong effect on their relative widths.

Finally we have also obtained results for the $n=3$ cross sections. We find these to be of the order of 3% of the main channel in a 20-eV broad region above threshold. The $3p$ channels dominate near threshold while the $3s$ channel becomes the stronger one at higher energies.

ACKNOWLEDGMENTS

This work was supported by a grant from the U.S. National Science Foundation. One of us (S.S.) wants to thank the Swedish Natural Science Research Council for support. A generous computing grant from the University of Virginia is also acknowledged. We are grateful to Dr. Z. Altun and Raymond Simons for helpful discussions.

*Present address: Department of Physics, Chalmers University of Technology, S-412 96 Göteborg, Sweden.

[1]F. Wuilleumier and M. O. Krause, Phys. Rev. A **10**, 242 (1974).
[2]F. J. Wuilleumier, Ann. Phys. (Paris) **4**, 231 (1982).
[3]J. A. R. Samson, Phys. Rev. Lett. **22**, 693 (1969).
[4]M. O. Krause and F. Wuilleumier, J. Phys. B **5**, L143 (1972).
[5]J. M. Bizau, F. Wuilleumier, P. Dhez, D. L. Ederer, T. N. Chang, S. Krummacher, and V. Schmidt, Phys. Rev. Lett. **48**, 588 (1982).
[6]V. Schmidt, H. Derenbach, and R. Malutzki, J. Phys. B **15**, L523 (1982).
[7]D. A. Shirley, P. H. Kobrin, D. W. Lindle, C. M. Truesdale, S. H. Southworth, U. Becker, and H. G. Kerkhoff, in *X-Ray and Atomic Inner-Shell Physics (University of Oregon, Eugene, Oregon)*, Proceedings of the International Conference on X-Ray and Atomic Inner-Shell Physics—1982, AIP Conf. Proc. No. 94, edited by B. Crasemann (AIP, New York, 1982), pp. 569–583.
[8]D. W. Lindle, T. A. Ferrett, U. Becker, P. H. Kobrin, C. M. Truesdale, H. G. Kerkhoff, and D. A. Shirley, Phys. Rev. A **31**, 714 (1985).
[9]P. R. Woodruff and J. A. R. Samson, Phys. Rev. Lett. **45**, 110 (1980).
[10]P. R. Woodruff and J. A. R. Samson, Phys. Rev. A **25**, 848 (1982).
[11]E. E. Salpeter and M. H. Zaidi, Phys. Rev. **125**, 248 (1963).
[12]V. L. Jacobs and P. G. Burke, J. Phys. B **5**, L67 (1972).
[13]T. N. Chang, J. Phys. B **13**, L551 (1980).
[14]K. A. Berrington, P. G. Burke, W. C. Fon, and K. T. Taylor, J. Phys. B **15**, L603 (1982).
[15]J. A. Richards and F. P. Larkins, J. Electron Spectrosc. Relat. Phenom. **32**, 193 (1983).
[16]P. Scott and P. G. Burke, J. Phys. B **17**, 1321 (1984).
[17]S. Ormonde, W. Whitaker, and L. Lipsky, Phys. Rev. Lett. **19**, 1161 (1967).
[18]P. G. Burke and A. J. Taylor, J. Phys. B **2**, 44 (1969).
[19]R. S. Oberoi, J. Phys. B **5**, 1120 (1972).
[20]K. T. Chung, Phys. Rev. A **6**, 1809 (1972).
[21]D. R. Herrick and O. Sinanoğlu, Phys. Rev. A **11**, 97 (1975).
[22]V. S. Senashenko and A. Wagué, J. Phys. B **12**, L269 (1979).
[23]Y. K. Ho, J. Phys. B **12**, 387 (1979).
[24]Y. K. Ho, J. Phys. B **15**, L691 (1982).
[25]S. M. Burkov, N. A. Letyaev, S. I. Strakhova, and T. M. Zajac, J. Phys. B **21**, 1195 (1988).
[26]R. P. Madden and K. Codling, Astrophys. J. **141**, 364 (1965).
[27]R. P. Madden and K. Codling, Phys. Rev. Lett. **10**, 516 (1963).
[28]S. Salomonson, S. L. Carter, and H. P. Kelly, J. Phys. B **18**, L149 (1985).
[29]A.-M. Mårtensson, J. Phys. B **12**, 3995 (1979).
[30]E. R. Brown, S. L. Carter, and H. P. Kelly, Phys. Rev. A **21**, 1237 (1980).
[31]U. Fano and J. W. Cooper, Rev. Mod. Phys. **40**, 441 (1968).
[32]See A. L. Fetter and J. D. Walecka, *Quantum Theory of Many-Particle Systems* (McGraw-Hill, New York, 1971), pp. 59–64.
[33]M. Ya. Amusia and N. A. Cherepkov, Case Stud. At. Phys. **5**, 47 (1975).
[34]K. A. Brueckner, Phys. Rev. **97**, 1353 (1955); *The Many Body Problem* (Wiley, New York, 1959), pp. 47–241.
[35]J. Goldstone, Proc. R. Soc. London, Ser. A **239**, 267 (1957).
[36]H. P. Kelly, Adv. Theor. Phys. **2**, 75 (1968).
[37]I. Lindgren and J. Morrison, *Atomic Many-Body Theory*, 2nd ed., Vol. 3 of *Springer Series on Atoms and Plasmas*, edited by G. Ecker, P. Lambropoulus, and H. Walther (Springer-Verlag, Berlin, 1986).
[38]S. Garpman, I. Lindgren, J. Lindgren, and J. Morrison, Phys. Rev. A **11**, 758 (1975).
[39]I. Lindgren, J. Lindgren, and A.-M. Mårtensson, Z. Phys. A **279**, 113 (1976).
[40]I. Lindgren and S. Salomonson, Phys. Scr. **21**, 335 (1980).
[41]A.-M. Mårtensson and S. Salomonson, J. Phys. B **15**, 2115 (1982).
[42]L. M. Frantz, R. L. Mills, R. G. Newton, and A. M. Sessler, Phys. Rev. Lett. **1**, 340 (1958); B. A. Lippman, M. H. Mittleman, and K. M. Watson, Phys. Rev. **116**, 920 (1959); R. T. Pu and E. S. Chang, *ibid.* **151**, 31 (1966); H. J. Silverstone and M.-L. Yin, J. Chem. Phys. **49**, 2026 (1968); S. Huzinaga and C. Arnau, Phys. Rev. A **1**, 1285 (1970).

[43]A. F. Starace, in *Corpuscles and Radiation in Matter I,* Vol. 31 of *Handbüch der Physik,* edited by W. Mehlhorn (Springer-Verlag, Berlin, 1982), pp. 1–121.
[44]S. L. Carter and H. P. Kelly, Phys. Rev. A **24**, 170 (1981).
[45]J. W. Cooper, U. Fano, and F. Prats, Phys. Rev. Lett. **10**, 518 (1963).
[46]J. Macek, J. Phys. B **1**, 831 (1968).
[47]C. D. Lin, Phys. Rev. A **10**, 1986 (1974); **25**, 76 (1982).
[48]M. E. Kellman and D. R. Herrick, Phys. Rev. A **22**, 1536 (1980).
[49]S. Watanabe, M. Le Dourneuf, and L. Pelamourgues, J. Phys. (Paris) Colloq. **43**, C2-223 (1982).
[50]G. S. Ezra and R. S. Berry, Phys. Rev. A **28**, 1974 (1983).
[51]U. Fano, Phys. Rev. **124**, 1866 (1961).
[52]U. Fano and J. W. Cooper, Phys. Rev. **137**, A1364 (1965).
[53]L. Lipsky, in *V International Conference on the Physics of Electronic and Ionic Collisions* (Nauka, Leningrad, 1967), pp. 617–618.
[54]V. L. Jacobs, J. Phys. B **5**, 2257 (1972).
[55]D. Dill and U. Fano, Phys. Rev. Lett. **29**, 1203 (1972); U. Fano and D. Dill, Phys. Rev. A **6**, 185 (1972); D. Dill, *ibid.* **7**, 1976 (1973).
[56]J. Cooper and R. N. Zare, in *Atomic Collision Processes,* edited by S. Geltman, K. T. Mahanthappa, and W. E. Brittin (Gordon and Breach, New York, 1969), Vol. 11c, pp. 317–337.
[57]M. Ya. Amusia, N. A. Cherepkov, and L. V. Chernysheva, Phys. Lett. **40A**, 15 (1972).
[58]M. Ya. Amusia, N. A. Cherepkov, and L. V. Chenysheva, Zh. Eksp. Teor. Fiz. **60**, 160 (1971) [Sov. Phys.—JETP **33**, 90 (1971)].
[59]P. G. Burke, D. D. McVicar, and K. Smith, Phys. Rev. Lett. **11**, 559 (1963).
[60]P. G. Burke and D. D. McVicar, Proc. Phys. Soc. **86**, 989 (1965).
[61]T. F. O'Malley and S. Geltman, Phys. Rev. **137**, A1344 (1965).
[62]P. L. Altick and E. Neal Moore, Phys. Rev. Lett. **15**, 100 (1965); Phys. Rev. **147**, 59 (1966).
[63]L. Lipsky and A. Russek, Phys. Rev. **142**, 59 (1966).
[64]A. K. Bhatia, A. Temkin, and J. F. Perkins, Phys. Rev. **153**, 177 (1967); A. K. Bhatia and A. Temkin, *ibid.* **182**, 15 (1969); A. K. Bhatia, P. G. Burke, and A. Temkin, Phys. Rev. A **8**, 21 (1973); **10**, 459(E) (1974); A. K. Bhatia and A. Temkin, *ibid.* **11**, 2018 (1975); **29**, 1895 (1984).
[65]P. G. Burke and A. J. Taylor, Proc. Phys. Soc. **88**, 549 (1966); P. G. Burke, in *Invited Papers of Fifth International Conference on the Physics of Electronic and Atomic Collisions, Leningrad, 1967,* edited by L. Branscomb (University of Colorado, Boulder, 1968), p. 128.
[66]V. V. Balashov, S. I. Grishanova, I. M. Kruglova, and V. S. Senashenko, Phys. Lett. **27A**, 101 (1968); Opt. Spectrosc. (USSR) **28**, 466 (1970).
[67]L. Lipsky and M. J. Coneely, Phys. Rev. A **14**, 2193 (1976).
[68]L. Lipsky, R. Anania, and M. J. Coneely, At. Data Nucl. Data Tables **20**, 127 (1977).
[69]H. Doyle, M. Oppenheimer, and A. Dalgarno, Phys. Rev. A **11**, 909 (1975).
[70]G. W. F. Drake and A. Dalgarno, Proc. R. Soc. London, Ser. A **320**, 549 (1971).
[71]K. T. Chung and I. Chen, Phys. Rev. Lett. **28**, 783 (1972).
[72]A. P. Hickman, A. D. Isaacson, and W. H. Miller, Chem. Phys. Lett. **37**, 63 (1976).
[73]Y. K. Ho, Phys. Rev. A **23**, 2137 (1981).
[74]K. T. Chung and B. F. Davis, Phys. Rev. A **26**, 3278 (1982); **31**, 1187 (1985).
[75]E. McGreevy and A. L. Stewart, J. Phys. B **10**, L527 (1977).
[76]P. C. Ohja, J. Phys. B **17**, 1807 (1984).
[77]D. H. Oza, Phys. Rev. A **33**, 824 (1986).
[78]H. D. Morgan and D. L. Ederer, Phys. Rev. A **29**, 1901 (1984).
[79]C. L. Pekeris, Phys. Rev. **126**, 143 (1962); **126**, 1470 (1962); **127**, 509 (1962).
[80]F. Wuilleumier, M. Y. Adam, N. Sandner, and V. Schmidt, J. Phys. (Paris) Lett. **41**, L373 (1980).
[81]J. Jiménez-Mier, C. D. Caldwell, and D. L. Ederer, Phys. Rev. Lett. **57**, 2260 (1986).
[82]U. Fano and J. Macek, Rev. Mod. Phys. **45**, 553 (1973).
[83]P. Dhez and D. L. Ederer, J. Phys. B **6**, L59 (1973).
[84]D. W. Lindle, P. A. Heimann, T. A. Ferrett, and D. A. Shirley, Phys. Rev. A **35**, 1128 (1987).